SAND2017-11231C

Properties of Brines formed by Deliquescence of Sea-Salt Aerosols

C. R. Bryan[1], E.J. Schindelholz[2]
[1]Storage and Transportation Technologies Department
[2]Materials Reliability Department
Sandia National Laboratories
Albuquerque, NM 87185
U.S.A.

ABSTRACT

For long-term dry storage, most spent nuclear fuel in the United States is placed in welded 304 or 316 stainless steel canisters that are stored within passively ventilated overpacks. As the canisters cool, sea-salt aerosols deposited on the canister surfaces will deliquesce to form potentially corrosive brines. We have used thermodynamic modeling to predict the chemical composition of the brines that form by deliquescence of sea-salt aerosols, and to estimate brine volumes and salt/brine volume ratios as a function of temperature and atmospheric relative humidity. We have also mixed representative brines and measured the physical and electrochemical properties of those brines over a range of temperatures. These data provide a matrix that can be used to predict the evolution of deliquescent brine properties over time on storage canister surfaces, as the canisters cool and surface relative humidity increases. Brine volumes and properties affect corrosion kinetics and damage distributions on the metal surface, and may offer important constraints on the expected rate and extent of corrosion and the timing of SCC crack initiation. The predicted brines do not consider reactions with atmospheric gases that are known to affect sea-salt particle and deliquescent brine compositions under field conditions. The potential effects of such reactions are discussed, and preliminary modeling and experimental data are presented.

Key words: seawater; aerosol; deliquescence; brine; spent nuclear fuel; dry storage canisters

INTRODUCTION

In the United States, spent nuclear fuel (SNF) from nuclear power reactors is eventually moved from storage pools to dry storage at near-reactor Independent Spent Fuel Storage Installations (ISFSIs). Typically, the dry storage systems are welded stainless steel (304 or 316) containers enclosed in concrete, or steel and concrete, overpacks[1]. For most dry storage systems, passive ventilation is used to cool the canisters within the overpacks, and large volumes of outside air are drawn through the system by natural convection. Inherent in this passive design is the potential for dust and aerosols within the air to be deposited on the steel canisters, and, as the casks cool over time, salts in the dust will deliquesce (absorb water) to form brine on the storage container surface. If the salts contain aggressive components such as chloride, localized attack can occur. Most modes of corrosion, including general corrosion, pitting, and crevice corrosion, cannot significantly damage the steel canisters within anticipated storage times. However, one corrosion mechanism, chloride-induced stress corrosion cracking (SCC), may propagate relatively rapidly under some conditions and could potentially result in canister penetration during long-term interim storage. Chloride-induced SCC is a well-documented mode of attack for stainless steels (including 304SS and 316SS) in marine environments[2], and many ISFSIs are in coastal areas.

In near-marine settings, chloride-rich sea-salts generated by wave action and evaporation of sea-spray can comprise a large fraction of the atmospheric aerosols present, and can be deposited on the canister

surface. As the fuel radioactivity decreases and less heat is generated, canister surface temperatures drop and the salts will deliquesce to form potentially corrosive chloride-rich brines on the canister surface. The occurrence of sea-salt aerosols on SNF dry storage canisters has been confirmed, when sea-salt aggregates were observed in dust samples collected from canister surfaces at the Diablo Canyon ISFSI[3,4].

Once a brine is present on the canister surface, the corrosion can begin. However, over time, the brine volume, composition, and properties change, as deposited salt loads increase and the canister continues to cool, resulting in a rise in the surface relative humidity (RH). Brine layer properties control the distribution and size of the cathode around a corrosion pit and limit the maximum cathodic current that can be produced[5], thus affecting corrosion kinetics, damage distributions, and the extent of corrosion (e.g., maximum pit depth) on the metal surface. Pitting initiation and growth will in turn affect the timing of SCC crack initiation[6-8]. Hence, understanding the evolution of brine properties as a function of the evolving canister surface environment (RH, temperature, and salt load) is necessary to improve predictive models for long-term canister corrosion performance.

To do this, we have implemented standard thermodynamic modeling to determine the composition of brines formed by sea-salt deliquescence, as a function of RH and temperature. We then mixed brines to represent specific RH values, and characterized those brines, measuring conductivity and density. The theoretical and experimental data were used to calculate brine volumes and brine-to-salt volume ratios as a function of RH and salt load. These data provide insights into structure and composition of deliquescent brines and the potential limits on the extent of atmospheric corrosion on heated metal surfaces.

THERMODYNAMIC MODELING OF BRINES FORMED BY SEA-SALT DELIQUESCENCE

Sea-salt aerosols reflect the composition of sea water, the typical composition of which is represented by ASTM substitute seawater[9], shown in Table 1. Dominant ions in seawater are Na^+ and Cl^- with lesser amounts of Mg^{2+}, Ca^{2+}, K^+, and SO_4^{2-}. Sea spray evaporates to form more and more concentrated solutions, eventually converting to dry salts. These salts, upon deliquescence, follow the evaporation pathway in reverse, initially forming highly concentrated chloride-rich brines, and progressively become more and more dilute. At equilibrium, the activity of water (a_w) in a brine is equal to the activity of water in the atmosphere above the brine, which is equal to the relative humidity (RH), expressed as a unit value. Evaporation is simply the inverse of deliquescence, and the composition of brines formed by sea-salt deliquescence, as a function of the a_w in the brine can be predicted by modeling the evolution of seawater as it evaporates. Here, the compositional evolution of evaporating sea water was modeled using the thermodynamic solubility and speciation modeling program EQ3/6[10] and the Yucca Mountain Program Pitzer database.[11] The Yucca Mountain Pitzer database was specifically developed to evaluate the composition of concentrated salt solutions formed by evaporation, and has been thoroughly validated for that use. The starting water for the calculations was ASTM simulated seawater, and equilibrium with atmospheric CO_2 ($10^{-3.33}$ bars) was assumed. Brine compositions were evaluated from 10°C to 80°C, at RH values from that representing equilibrium with unevaporated seawater (RH = 98.15%) to the lowest value possible. Brine compositions for RH values below the deliquescence point of bischofite ($MgCl_2{:}6H_2O$) are discussed, but are speculative.

Table 1.

Typical composition of seawater[9]

Species	Na^+	K^+	Mg^{2+}	Ca^{2+}	Cl^-	Br^-	F^-	SO_4^{2-}	BO_3^{3-}	HCO_3^-	pH
mg/L	11031	398	1328	429	19835	68	1.4	2766	25.7	146	8.2

Model predictions for seawater evaporation at 25ºC are shown in Figure 1. In Figure 1a, solute concentrations are plotted against RH (a_w × 100). Inflections in the concentration curves occur when a mineral phase begins to precipitate, even if that mineral phase does not contain the species of interest. In **Figure 1**b, the concentrations are given in terms of concentration factor (CF), calculated as (original water mass)/(remaining water mass). On the concentration factor plot, solutes plot along a straight line as long as they are conserved in solution. During evaporation, brines are dominantly Na+ and Cl^- rich until halite precipitates at 73% RH (CF of 11), and evolve towards Mg^{2+}-Cl^- brines until bischofite ($MgCl_2$:$6H_2O$) precipitates at 36% RH (CF of 222); at this point, the brine is almost entirely $MgCl_2$. The thermodynamic model predicts brine below this RH, because B and Br are conserved in solution—that is, no mineral containing them is predicted to precipitate. However, the YMP database is not qualified for use to predict borate species and contains few borate salts, so the enrichment in B may not be real. Moreover, as Br concentrations in evaporating seawater go up, it is incorporated into halite as a trace component. It is not clear that a free brine will exist below the deliquescence RH of bischofite.

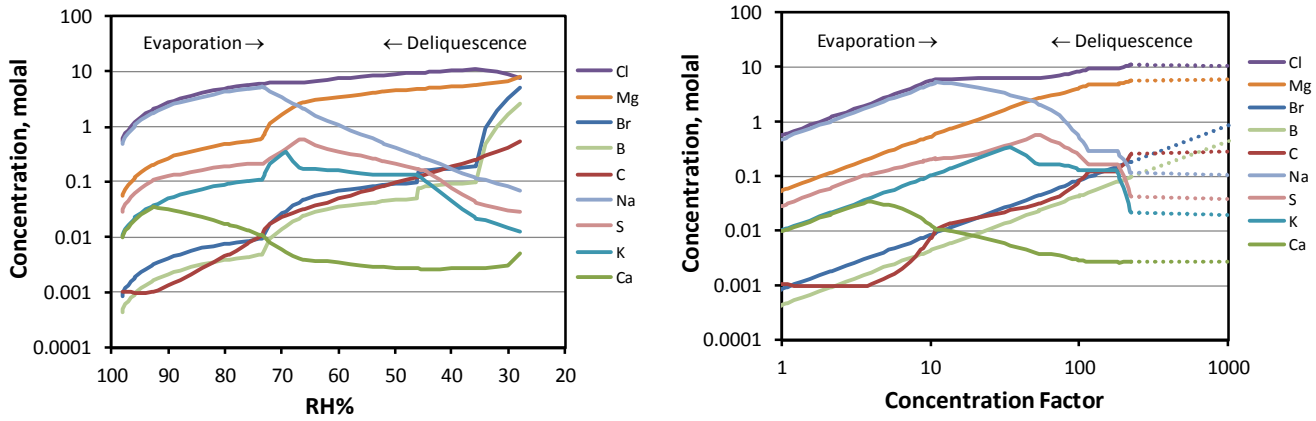

Figure 1: Evaporation of seawater. (a) Predicted brine composition as a function of RH. (b) Predicted brine composition as a function of concentration factor.

Mineral precipitation ultimately controls the relative proportion of species in the evaporating brine. Salt minerals that are predicted to precipitate out during evaporation are shown in Figure 2. In order of occurrence, calcite ($CaCO_3$) precipitates first, and then gypsum ($CaSO_4$:$2H_2O$), which converts to Anhydrite ($CaSO_4$) at a concentration factor of about 9. Halite (NaCl) precipitates at a concentration factor of about 11. Other minerals precipitate, and in many cases re-dissolve, as the seawater evaporates. The final salt assemblage at dry-out consists mostly of halite, with minor amounts of Bischofite ($MgCl_2$:$6H_2O$) and Kieserite ($MgSO_4$:$2H_2O$) and trace amounts of Anhydrite, Carnallite ($KMgCl_2$:$6H_2O$), and Hydromagnesite ($Mg_5(CO_3)_4(OH)_2$:$4H_2O$). Note that magnesite ($MgCO_3$) is the thermodynamically stable magnesium carbonate, but has been suppressed in the thermodynamic calculation. This was done because magnesite is kinetically inhibited from nucleating, and is rarely observed to form at temperatures below 100ºC. However, precipitation of $MgCO_3$ has occasionally been achieved at low temperatures, and may be enhanced by cyclic changes in the environment,[12,13] such as diurnal changes in temperature and RH. The identity of the magnesium carbonate phase that precipitates has little effect on the predicted brine compositions.

As sea-spray aerosols dry out, these salts are precipitated, and salts, or a mixture of salts and brine, may be deposited on the canister surface. As the RH rises over time, the salts re-dissolve and the composition of the deliquescent brine follows the path of evaporation in reverse order. It is the highly deliquescent $MgCl_2$:$6H_2O$ that is believed to control the deliquescence behavior of sea salts; determining when an aqueous phase is present.

Seawater evaporation was modeled at temperatures from 10ºC to 80ºC, and the predicted brine compositions do not vary greatly. The largest effect of temperature is on the deliquescence point of bischofite, which shifts from 36% to 28% RH with increasing temperature, and on the identity and

deliquescence point of the ternary and quaternary salts that precipitate out between 45 and 50% RH. The deliquescence point of halite at 74% RH is nearly independent of temperature.

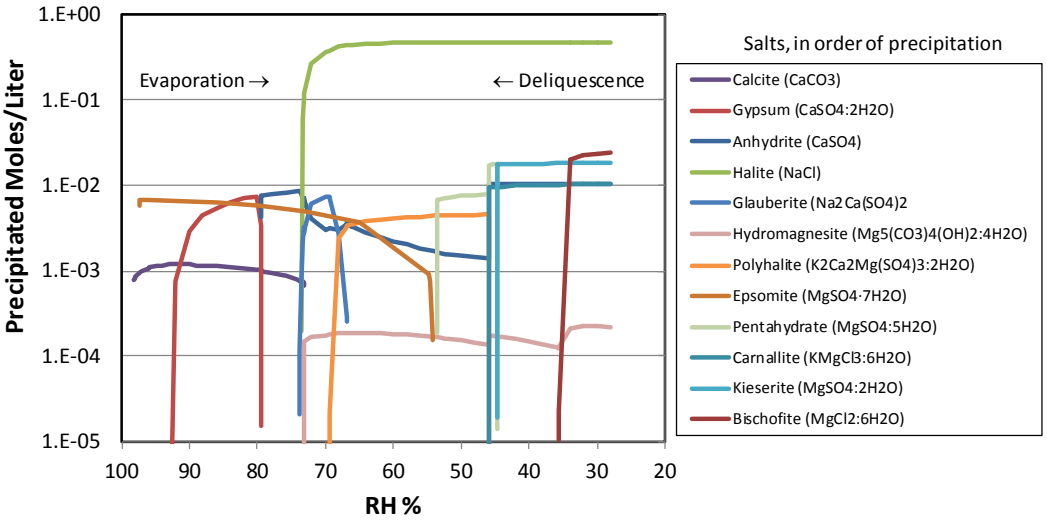

Figure 2: Evaporation of Seawater. Predicted salt phases as a function of concentration factor.

The thermodynamic modeling also provides other data that is important for modeling corrosion processes in relevant brines and at relevant canister surface temperatures. One parameter of interest is the dissolved oxygen concentration in the brines, as that potentially affects the kinetics of the oxygen reduction reaction (ORR) at the cathode on the metal surface surrounding the corroding pit or crack. Calculated oxygen solubilities in the deliquescent brines, assuming equilibrium with the Earth's atmosphere, are shown in Figure 3 as a function of temperature and equilibrium RH (a_w in the brine). At all temperatures, oxygen solubilities are highest in unevaporated sea-water, and decrease as the water evaporates and concentrates. Above the deliquescence point of NaCl (~4% RH) increasing temperature results in a decrease in oxygen concentration; however, at lower RH values, where sodium precipitates out and the brine becomes progressively more magnesium-rich, the trend is reversed—oxygen concentrations increase with increasing temperature.

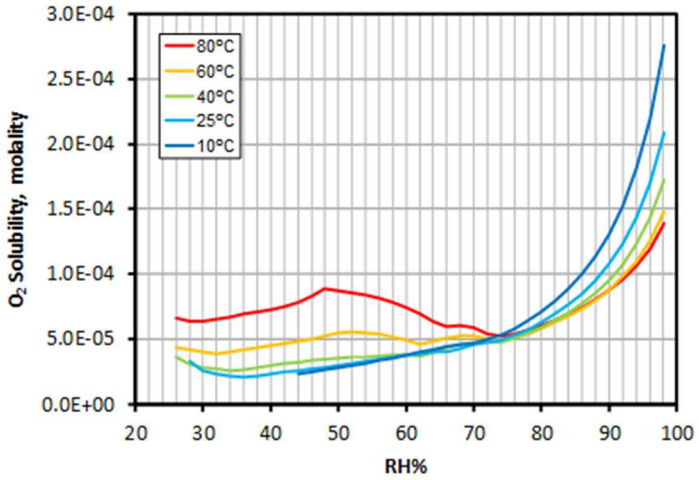

Figure 3. Calculated oxygen solubilities in brines formed by sea-salt deliquescence, as a function of temperature and RH.

If correct, these calculations suggest the following for corrosion under thin films:

- For relatively thick brine films, when oxygen diffusion through the film limits the rate of ORR at the metal surface, lower solubilities in brines representing less than 74% RH should slow oxygen diffusion rates and reduce cathode kinetics.
- As brine films thin, oxygen diffusion eventually ceases to be the limiting process for ORR. In concentrated brines (<74% RH) thinner films will be required before oxygen diffusion ceases to be limiting.
- The effect of temperature is complex. Higher temperatures support more rapid diffusion, but oxygen solubilities show a complex relationship with temperature and brine composition.

As sea-salts deliquesce (or sea-water evaporates), the volume of brine present changes. For a given mass of sea-salt aerosol particles, we can use the thermodynamic model to calculate the volume of the brine and of the precipitated salts as a function of RH and of salt surface load. Moreover, if it is assumed that the brine is distributed as a continuous film across the surface, then a brine film thickness can be calculated. This assumption requires redistribution of salts on the canister surface from discrete deposited particles to a uniform layer, and is unproven. However, performing this calculation provides insights into the RH and temperature dependence of the brine volume, and the potential importance of processes dependent upon brine film thickness. The calculation of brine layer thickness requires brine density as a function of composition and temperature; estimation of these values is described later.

Figure 4a shows predicted brine layer thicknesses, assuming a continuous film at 25ºC, as a function of RH and salt load. The thickness dependence on RH is the same for all salt loads, as for a given set of conditions (T and RH), brine layer thickness varies linearly with salt load. Inflections in each curve represent RH conditions at which a salt mineral precipitates. In each case, the layer thickness decreases by about a factor of 10 as the RH is reduced from 98% (unevaporated sea-water) to 74%, where NaCl precipitates. The brine thickness decreases an additional order of magnitude as the RH drops to about 46%, where carnallite precipitates. Below this RH, the brine is nearly pure magnesium chloride. Bischofite precipitates at 36% HR (at 25ºC); as discussed earlier, predicted brine thicknesses below that RH probably reflect limitations of the thermodynamic database with respect to B and Br. An important point is that oxygen diffusion through the brine layer is not anticipated to be limiting with respect to the oxygen reduction reaction at brine films thinner than 20 μm[14], and calculated brine layer thicknesses below the deliquescence point of NaCl are consistently below this, even for relatively high salt loads. Moreover, the predicted thicknesses are so small that development of a continuous brine film through sea-salt aerosol deliquescence alone seems unlikely.

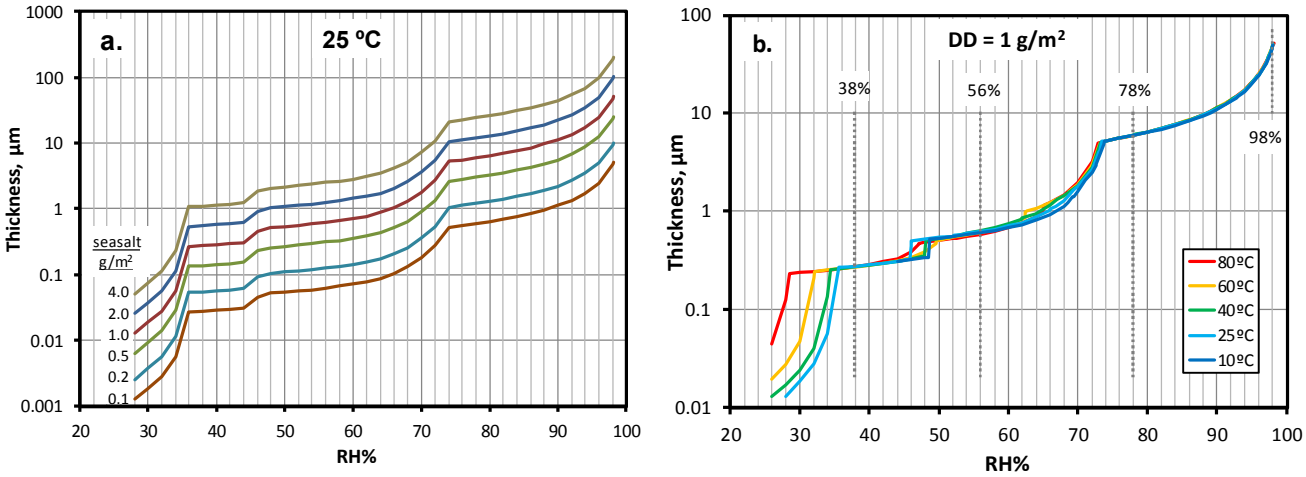

Figure 3. Calculated Brine Layer thicknesses, as a function of RH and (a) salt load, and (b) temperature.

Calculated brine layer thicknesses as a function of temperature are shown in Figure 4b. Temperature has a relatively minor effect on the predicted brine volumes. There is a small step when carnallite precipitates at around 45% RH, and this value varies slightly with temperature. The other major change is in the deliquescence point of bischofite, which shifts to lower values with increasing temperature.

As sea-salts deliquesce, it is perhaps not obvious how the actual amount of brine present compares to the total volume of solid salts present. This information is useful in assessing the degree of continuity in the brine layer that might form by deliquescence of small (generally ~10 µm) sea-salt aerosols. To assess this, brine and precipitated salt masses predicted by the thermodynamic modeling were combined with estimates of brine density and known mineral densities to calculate brine and precipitated solid volumes. Then, the brine-to-solids volume ratio was calculated as a function of RH. The results are shown in Figure 4. At RH values above the deliquescence point of NaCl, brine volumes are orders of magnitude greater than the precipitated salts, which consist only of small amounts of calcite and gypsum (Figure 2). At RH values below 74%, brine volumes decrease rapidly as NaCl precipitates. At 60% RH, brine and precipitated salts are about equal in volume. Carnallite precipitates at 45-50% RH; at lower RH values, the brine/salt volume ratio is in the range of 0.4 to 0.3. Upon initial deliquescence of bischofite, a typical sea-salt aerosol particle, about 10 µm in diameter, would produce a small pool of magnesium chloride about 1/3 the volume of the remaining precipitated solids.

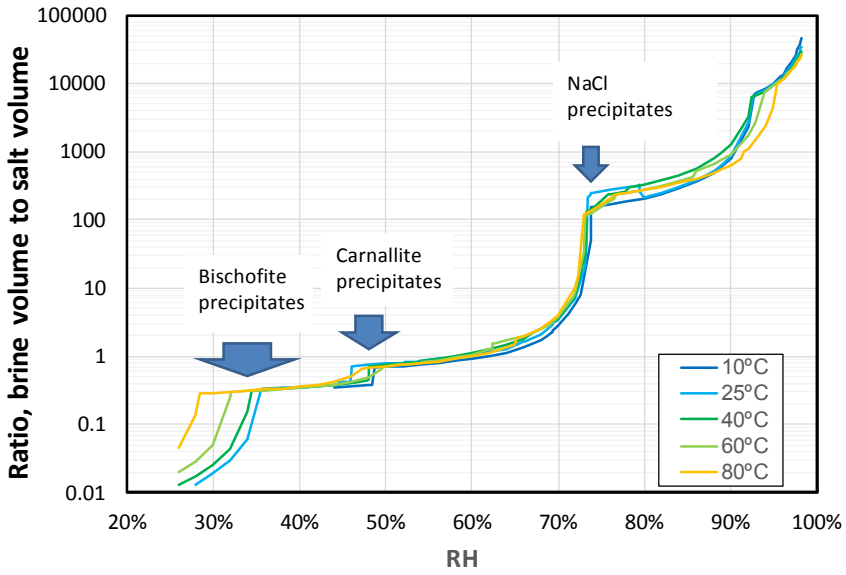

Figure 4. Brine/salt volume ratio dependence on RH.

EXPERIMENTAL MEASUREMENT OF BRINE PROPERTIES

As discussed previously, to estimate brine volumes, brine densities were necessary. An additional brine property that is necessary to know for mechanistic pitting models[5] is brine conductivity. To estimate these values, four brine compositions along the predicted evolutionary pathway for seawater evaporation at 25ºC (Figure 1) were mixed using ACS certified salts. The brines correspond to 98.15% RH (unevaporated seawater); 78% RH, 56% RH, and 38% RH. They were chosen to represent regions far from mineral precipitation events, where the brine composition has little temperature dependence (Figure 3b). Because there is relatively little temperature dependence, these brines, predicted for 25ºC, are good analogs for higher-temperature brines at the same RH values. The compositions of the four brines are provided in Table 2. It should be noted that the fact that these brines can be mixed in the exact compositions predicted provides a certain level of validation for the thermodynamic model.

Table 2.

Composition of Brines Used for Experimental Testing

Brine RH	Species Concentration (molality)									
	Na^+	K^+	Mg^{2+}	Ca^{2+}	Cl^-	Br^-	F^-	SO_4^{2-}	BO_3^{3-}	HCO_3^-
98% (SW)	0.498	0.011	0.057	0.011	0.580	0.001	0.0001	0.030	0.001	0.002
78%	4.507	0.096	0.513	0.015	5.250	0.008	—	0.196	0.004	0.006
56%	0.719	0.144	3.907	0.003	7.941	0.077	—	0.289	0.040	0.064
38%	0.145	0.032	5.500	0.003	10.610	0.181	—	0.059	0.093	0.215

Once mixed, conductivity was measured using a conductivity meter with a maximum working temperature of 80ºC. The cited range of the conductivity probe used for the test is 0-150 mS/cm, but testing showed that the response was accurate and linear up to 200 mS. For each brine, data were collected over the temperature range for which the conductivity was less than 200 mS/cm. For any given brine, measured conductivities increase linearly as a function of temperature (Figure 5a), so these data can be used to estimate brine conductivities at higher temperatures, when the range of the probe is exceeded. Measured and estimated conductivities from 10ºC to 80ºC are shown in Figure 5b. Note that the brine corresponding to 74% RH (the deliquescence RH for halite in this salt mixture) was not mixed, and the data points shown in Figure 5b at that RH are inferred indirectly from trends in conductivity with composition. While solution concentration (ionic strength) increases consistently as the RH decreases (as it must), conductivity shows a more complex response. At high RH (e.g., seawater), ionic strength and conductivity are both low. As the RH drops and the solution becomes more concentrated, the conductivity increases, reaching a maximum at the point of halite deliquescence, when the solution concentration is approximately 6 molal sodium chloride. As the RH decreases further, the brine becomes more and more magnesium-rich and the conductivity drops; this is consistent with anticipated behavior of divalent cation-rich brines.[15] At 38% RH, the conductivity is only $^1/_3$ to $^1/_2$ of the maximum value at 74% RH; it would be even lower at the RH of bischofite deliquescence.

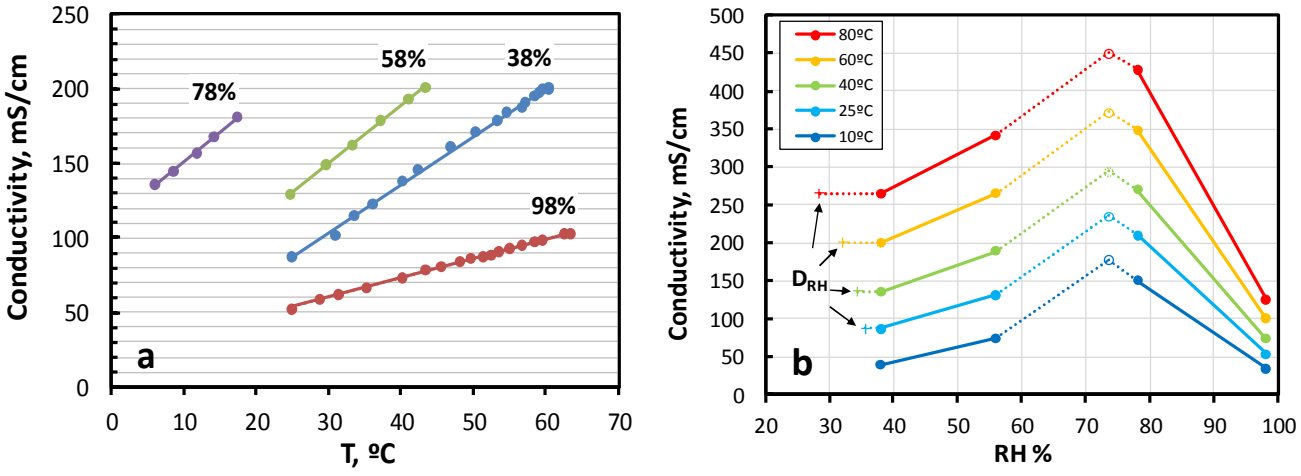

Figure 5. Conductivity of representative sea-salt deliquescent brines. (a) measured values; (b) measured and estimated values, as a function of temperature.

As noted previously, brine densities are necessary for calculating brine layer thicknesses from the thermodynamic model data. They were measured for the brines of interest using hydrometers calibrated for specific gravity ranges from 1.000 to 1.220, and 1.20 to 1.420 (density and specific gravity differ by

less than 0.01%). The hydrometers were calibrated for temperatures of 60ºF (15ºC) and a slight error is introduced at other temperatures. To verify their use, the density of saturated NaCl solutions was measured over a range of temperatures, and the values compared to known values[16]; measurement errors were less than 0.003 units. Using the hydrometers, the densities of the four test brines were measured up to 65ºC (Figure 6). Brine densities decrease with temperature, but the change is small.

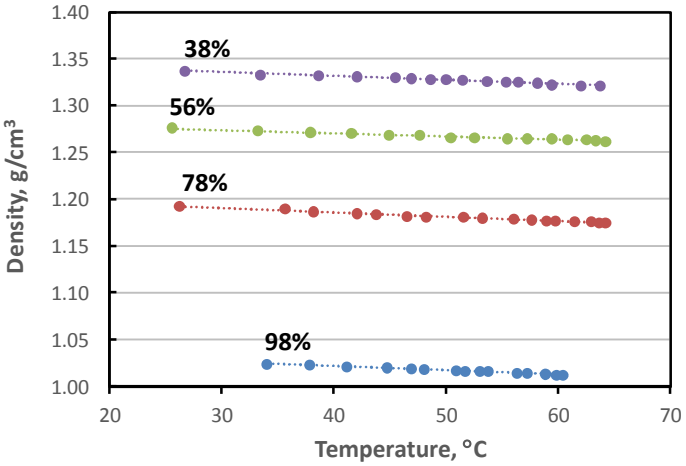

Figure 6. Measured brine densities.

Using brines predicted to form by evaporation at 25ºC to estimate brine properties at higher temperatures introduces some error in the predicted density and conductivity values. This was done because it is difficult to mix the higher temperature brines and to store them; they are unstable at lower temperatures, precipitating out salts as they cool. The error is negligible for the 98% and 78% brines because the brine compositions show little dependence on temperature. However, as RH values drop below the point of halite saturation, the 25ºC compositions vary increasingly from the predicted high-temperature brines at those RH values. For instance, at 38% RH, the predicted brine composition changes from 5.5 molal Mg and 10.6 molal Cl at 25ºC, to 5.8 molal Mg and 11.7 molal Cl at 80ºC. This will have some effect on brine densities, especially for the 38% brine. Because of the higher salt load, the densities for those brines will be higher than predicted in Figure 6 and the density may increase slightly with temperature, rather than decreasing. However, the effect on predicted brine layer thicknesses will be small, no more than 1-2%. The potential error in conductivity is likely to be greater; given the overall trend of decreasing conductivity with increasing magnesium content, values in Figure 5 may over-predict conductivities in sea-salt deliquescent brines at elevated temperatures and low RH values.

The brine compositions and precipitated salt assemblages predicted here are consistent with previous thermodynamic modeling,[17,18] and with experimental studies of seawater evaporation dating back over 150 years.[19-23] The calculations represent evaporation of seawater or deliquescence of sea-salts in bulk amounts and at relatively low temperatures, and equilibrium with atmospheric gases present at constant and relatively high levels (O_2, CO_2) is assumed. However, any chloride-containing brine will generate a partial pressure of HCl, and if that partial pressure is greater than the partial pressure of the HCl in the atmosphere, then that brine will degas HCl. For bulk systems, reactions that can result in degassing of HCl can be ignored for two reasons: (1) in the absence of a buffering reaction, this process is self-limiting—as acid is degassed, the pH rises and the partial pressure of HCl decreases until it is equal to that in the local atmosphere and degassing stops; and (2) even if a buffering reaction does occur, the partial pressures of HCl that are generated are extremely low, so that a huge volume of air is necessary to sweep away any significant amount of chloride.

Unlike bulk systems, HCl degassing cannot be ignored for seasalt aerosols, because the total amount of chloride present is very small and surface areas for exchange with the atmosphere are very large. Moreover, several reactions with atmospheric gases can buffer the pH, allowing for continued

degassing of HCl. These include sea-salt aerosol reactions with strong inorganic acids such as HNO_3 and SO_2 (which reacts with water to form H_2SO_4):

$$NaCl(s, aq) + HNO_3(g) \leftrightarrow NaNO_3(s, aq) + HCl(g)$$

$$2NaCl(s, aq) + H_2O + ½O_2 + SO_2(g) \leftrightarrow Na_2SO_4(s) + 2HCl(g)$$

In addition, there are a number of photochemically-mediated reactions with nitrous oxides that can transfer chloride from the solid to the gas phase.[24] Because of these reactions, sea-salt aerosols even over the ocean are significantly depleted in chloride relative to seawater,[25] and as sea-salt aerosols in near-marine settings are blown inland, they become progressively enriched in nitrate and/or sulfate, with a concomitant loss of chloride.[26-28] The occurrence of such reactions is strongly site-specific, as nitric acid and SO_2 levels in the atmosphere vary widely.

With partially deliquesced sea-salts in contact with a magnesium-rich brine, a similar reaction can occur with CO_2, which acts as a weak acid, forming carbonic acid in solution. As CO_2 is absorbed and HCl degasses, the pH continues to rise until a carbonate mineral precipitates, at which point, the pH is buffered, and the solution composition becomes invariant:

$$Mg^{+2}(aq) + 2Cl^{-}(aq) + H_2O + CO_2(g) \rightarrow MgCO_3(s) + 2HCl(g)$$

If this reaction goes to completion, then the highly deliquescent magnesium chloride is replaced with non-deliquescent magnesium carbonate and the sea-salt brine will dry out, narrowing the RH range over which metal corrosion can occur. The reaction is strongly temperature-sensitive. At low temperatures, brine HCl partial pressures may be lower than ambient values, and HCl will be absorbed by the particles. However, at elevated temperatures, the brines degas HCl and absorb CO_2 to form the carbonate. The direction of the reaction is determined by the relative magnitudes of the ambient HCl partial pressure and that being generated by the brine, at the pH at which it is buffered by magnesium carbonate precipitation.

To evaluate this thermodynamically, the geochemical modeling program EQ3/6[10] and the Yucca Mountain Pitzer database[11] were used. We assume that this reaction can occur as soon as deliquescence occurs (or even before, if an adsorbed water film forms on the salt surface below the deliquescence RH); therefore Mg^{+2} and Cl^{-} concentrations were fixed to be at saturation with bischofite at the temperature of interest. The CO_2 gas concentration was set to the current atmospheric value of $10^{-3.4}$ bars. Mg-carbonate and bischofite stability fields were determined as a function of canister surface temperature and atmospheric HCl(g) concentration. The model results are shown in Figure 7; also shown are typical ranges for atmospheric HCl concentrations in marine, continental, and industrial settings.[29-33] It is assumed that dry salts will not react with atmospheric CO_2, so carbonation can only occur once brine is present. At an absolute humidity of 30 g/m^3 (a bounding value identified by examining weather data from stations near existing ISFSIs), the maximum temperature of bischofite deliquescence is about 51ºC. However, many studies have observed atmospheric corrosion of mild steel or stainless steel at values well below the deliquescence point of the chloride salts involved.[34-38] For 304 SS, corrosion at RH values as low as 15% has been observed.[34, 35] This reactivity is attributed to thin adsorbed water films on the salts, and implies that conversion to Mg-carbonate could also occur at these RH values. This raises the maximum temperature of reaction to about 70ºC.

The modeling indicates that higher HCl(g) partial pressures are generated by the brine at elevated temperatures, supporting degassing and formation of Mg-carbonate. As noted previously, magnesite is kinetically inhibited from precipitating in many environments, and the more soluble hydromagnesite precipitates. Stability fields for both are shown in Figure 7. Because hydromagnesite is more soluble, it does not precipitate until the pH has risen to a higher value, corresponding to a higher carbonate concentration in solution and a lower acid gas concentration—that is why the hydromagnesite stability field is shifted to lower P_{HCl} values. It is not clear, in concentrated $MgCl_2$ brines with low water activities, if magnesite or hydromagnesite would precipitate. Moreover, there are several other known Mg-carbonate minerals with varying numbers of waters of hydration and varying carbonate to hydroxide ratios, and even a Mg-carbonate-chloride phase, which were not evaluated here. Bischofite is the stable magnesium chloride phase over the temperature range of interest.

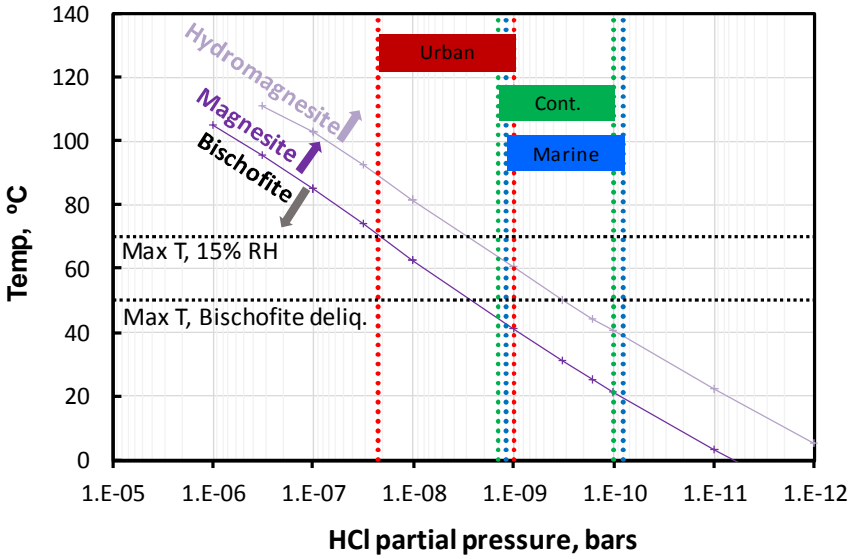

Figure 7. Calculated stability fields for bischofite and magnesium carbonate in T-P_{HCl} space.

It is important to note, also, that the HCl partial pressures that are generated by the brine as it degasses on the phase boundary are very low at relevant temperatures. For instance, if magnesite is the solubility limiting carbonate, then at 60ºC, the P_{HCl} would be only about 1×10^{-8} bars, corresponding to only about 14 µg/m^3 of air. If hydromagnesite is the precipitating phase, then the P_{HCl} is an order of magnitude lower, corresponding to 1.3 µg/m^3. These low capacities for chloride removal may limit the extent of degassing in laboratory settings where air flow rates are low; however, estimated air flow rates through interim storage canister overpacks are on the order of cubic meters per minute, and degassing should not be constrained by limited air volumes. However, the efficiency of HCl loss from the brine surface is also not known, and may be kinetically limiting.

The occurrence and rate of the magnesium chloride carbonation reaction was evaluated experimentally. To do this, magnesium chloride brine (1M, in 17% ethanol solution) was sprayed onto an inert substrate—polished silicon wafers 25 mm in diameter—using an ink-jet printer as described in Schindelholz and Kelly[40]. This deposition method produced randomly-spaced, isolated droplets of brine on the wafer surface; using dispersed droplets greatly increases the brine surface area-to-volume ratio, and increases the rate of exchange with the gas phase. This is realistic—the droplets are only slightly larger than sea-salt aggregates collected from in-use storage canisters at the Diablo Canyon ISFSI, which were ~10 µm in diameter[3]. For the experiment, the initial salt load was ~88 µg/sample $MgCl_2$ (17.4 µg/cm^2). After salt deposition, the wafers were stored in a nitrogen-purged cabinet until use. Three samples were retained to quantify the initial condition, and the remaining six samples were placed in a controlled-humidity chamber at 48º C and 40% RH, slightly above the deliquescence RH of bischofite (35% at that temperature). The atmosphere in the chamber was replaced at a rate of 2 L/min, using air that had been passed through an air cleaning system capable of removing all contaminants from the air stream. Three samples pulled after 30 days, and the final three after 69 days. All samples were stored in a nitrogen-purged cabinet until analysis.

To determine if partial or complete conversion to carbonate occurred, the samples were analyzed using Scanning Electron Microscopy (SEM) and Energy Dispersive X-ray Spectroscopy (EDS), Time-of-Flight Secondary Ion Mass Spectrometry (TOF-SIMS), and Raman spectroscopy. Finally, except for the samples for TOF-SIMS analysis, all samples were leached with deionized water, and the dissolved salts were analyzed by ion chromatography (IC). This yielded Mg and Cl concentrations, but not carbonate.

For SEM-EDS analysis, one 68-day sample was initially evaluated. A secondary electron (SE) image of the 68-day sample is shown in Figure 8. The image shows the distribution of the brine on the silicon wafer, occurring as randomly located, but non-overlapping droplets, varying in size from 10-25 μm in diameter. Originally present as liquid droplets in the humidity chamber, the droplets dried in the vacuum of the SEM, and occur in different morphologies. Most droplets (80-90%), dried to leave a smooth but wrinkled, “raisin-like” surface. The remainder dried to form rings with elevated edges and smooth centers; the ring-like drops are all in the smaller size range, although not all small drops show the ring structure. Element maps of the region imaged are also shown in Figure 18, and illustrate that there is a strong compositional control on droplet morphology; the ring-like droplets contain carbon, while the more abundant wrinkled droplets do not. The relationship between composition and droplet morphology was confirmed by EDS X-ray analysis. The carbonate-containing droplets have partially converted to Mg-carbonate, but still show large chloride peaks. Magnesium carbonates are much less deliquescent than magnesium chloride and would not be deliquesced at 40% RH. Hence, as the conversion progressed, the volume of brine in the droplet decreased, resulting in the formation of a flatter droplet upon drying. Moreover, the conversion to carbonate results in a large mass and volume loss in the dried salts, because the possible Mg-carbonates do not contain as much water as the bischofite.

Only the ring-like droplets show evidence of reaction; there is no carbon in the wrinkled droplets. It is not clear why this would occur, but there appears to be some relationship to droplet size. The largest droplets are never of the ring variety, and only a fraction of the mid-to-small droplets reacted. We speculate that surface tension effects associated with the higher radius of curvature for the smaller droplets results in a greater tendency to degas HCl. However, why only some droplets would be affected is not clear. Moreover, although SEM analysis of one 68-day sample showed clear signs of HCl degassing, TOF-SIMS analysis of a second sample indicated no evidence of carbonation, and subsequent examination of that sample by SEM also failed to show any evidence of carbonation. Raman spectroscopic analysis of the sample, did, however, indicate that carbonate was present in small amounts.

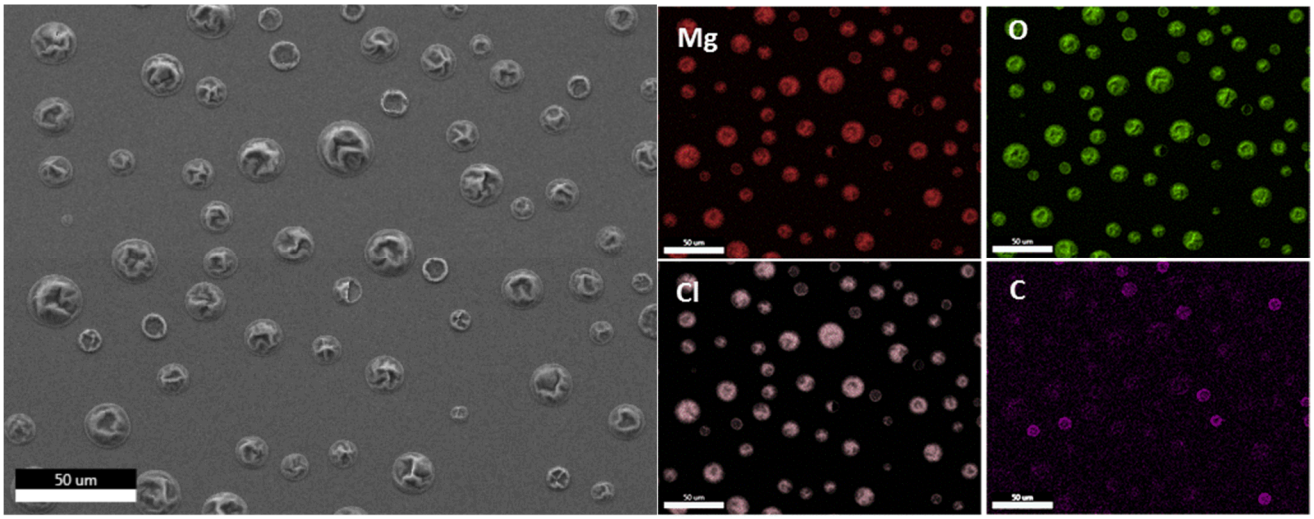

Figure 8. SEM image dried magnesium chloride droplets on a sample exposed for 68 days, illustrating the relationship between morphology and composition.

After retaining two samples (one untreated and on 68-day sample) for TOF-SIMS analysis, the salts were leached from all samples and analyzed by ion chromatography to verify chloride loss and to quantify the extent of the reaction. For all samples, only Mg and Cl were detected in quantifiable amounts, although Na, K, and ammonium were found in a few samples at trace concentrations. HCl degassing from the samples results in loss of chloride, but does not affect Mg concentrations. Hence,

the difference between the Mg^{2+} concentration and the Cl^- concentration in Equivalents is the amount of chloride that was lost by degassing. The percent of the initially-deposited chloride that was lost by degassing is plotted as versus equilibration time in Figure 9. Although the data are scattered, there is a trend of increasing chloride loss with exposure time, indicating that degassing occurred.

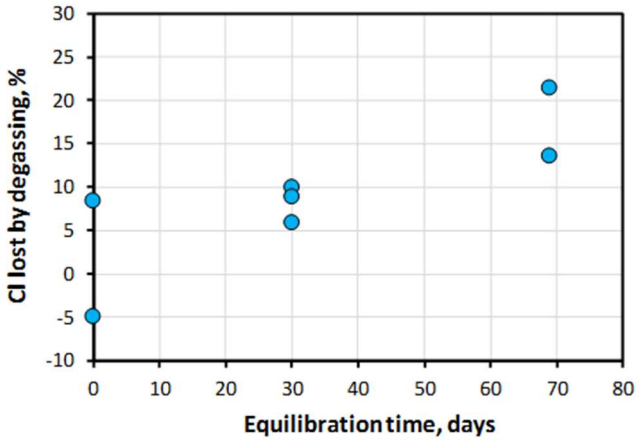

Figure 9. Fraction of Chloride Lost, as a Function of Equilibration Time.

The degassing process is kinetically limited; for the two samples analyzed after 69 days, the percent chloride lost was 13.6% and 21.5%. Only partial conversion was anticipated; at the HCl partial pressures predicted by the thermodynamic calculations for the temperature used, each cubic meter of air passing through the humidity chamber could only remove ~0.4 µg (hydromagnesite-buffered) to ~3 µg (magnesite-buffered) of chloride, assuming complete equilibration with the brine as the air flowed through the chamber. At the gas flow rate used (2 L/min) and the measured salt loadings (65.6 µg/sample), a single sample would take 15 days (magnesite) to 112 days (hydromagnesite) to fully degas. With six samples in the chamber for the first 30 days and three samples for the next 38 days, full degassing was not possible, even if complete equilibration between the headspace gas and the samples had occurred. No such limitation is present for magnesium chloride on a canister surface, because airflow through overpacks is on the order of cubic meters per minute, based on computational fluid dynamics calculations of heat-driven advection through the systems[39].

This experiment demonstrates that $MgCl_2$ brine at elevated temperatures can react with atmospheric CO_2 to degas HCl, converting to non-deliquescent magnesium carbonate. The experiment was specifically designed to promote degassing; HCl and other acid gas concentrations in the air stream were held at zero. For natural systems, carbonation will only occur if the ambient HCl concentration is less than that generated by the brine. The range of naturally occurring atmospheric HCl concentrations in marine, continental, and industrial areas is shown in Figure 7. Under natural conditions, carbonation can occur in the part of each range that is above the phase boundary, if magnesium chloride is deliquesced or at least has adsorbed surface water films. For the range of P_{HCl} values observed in marine and continental areas, carbonation could occur over a significant fraction of the range; in industrial areas, high ambient HCl partial pressures may inhibit carbonation. It is also important to note that as SNF storage canisters cool and surface temperatures drop, the reaction could reverse—the magnesium carbonate could absorb HCl and form a chloride-rich brine again.

Under natural conditions, other acidification reactions involving absorption of HNO_3 or SO_2 and degassing of chloride, or if ammonium salts are present, concomitant degassing of ammonia and HCl, might be more important, depending upon the partial pressures of the gas species in the atmosphere. However, the carbonation reaction described here may be critically important when considering experimental systems. Corrosion experiments are frequently carried out for very long times (months or years), and the total amount of $MgCl_2$ present as deposited salts may be small. Moreover, if experiments are run under “accelerated” conditions—using high temperatures and elevated RH values,

the possible degassing rate may be much higher. For example, for experiments carried out at 80ºC and 35% RH—conditions not possible in nature, but used in recent long-term corrosion experiments[35], the HCl partial pressure generated by the brine would by 30 times higher than in our experiment, requiring a much smaller volume of air to completely convert $MgCl_2$ to dry carbonates. Especially with experiments using sea-salts, where only a small fraction of the deposited salts is magnesium chloride, the possibility of carbonation and dry-out is real.

CONCLUSIONS

We have used thermodynamic modeling to predict the chemical composition of the brines that form by deliquescence of sea-salt aerosols, and to estimate brine volumes and salt/brine volume ratios as a function of temperature and atmospheric relative humidity. The brine volume calculations quantitatively illustrate that brines formed by deliquescence of sea-salt aerosols are unlikely to form by continuous films by deliquescence alone, although other forces may act to disperse the brines diffusion, capillary effects, etc.) on the metal surface. We have also mixed representative brines and measured the physical and electrochemical properties of those brines over a range of temperatures. Brine volumes and properties affect corrosion kinetics and damage distributions on the metal surface, and may offer important constraints on the expected rate and extent of corrosion and the timing of SCC crack initiation.

We have experimentally evaluated one such reaction, carbonation of magnesium chloride brines. This reaction is unlikely to occur at low temperatures, but is favored at elevated temperatures. Under SNF storage canister surface conditions, the carbonation reaction examined here may be of secondary importance relative to other acidification reactions. However, it may be critically important to planning and interpreting laboratory corrosion experiments, experiments may be carried out for months or years within controlled-atmosphere chambers. At lower temperatures, the stability of the corrosive chloride-rich brines that form in such chambers may be completely dependent on acid gas concentrations in the laboratory air entering the RH chamber. These gases are never measured or even considered, but may greatly affect experimental results, especially if the number of samples in the RH chamber is small and the salt load is light (limiting the amount of chloride present); or the experiment is run under “accelerated” (high temperature) conditions.

ACKNOWLEDGEMENTS

Sandia National Laboratories is a multimission laboratory managed and operated by National Technology and Engineering Solutions of Sandia, LLC., a wholly owned subsidiary of Honeywell International, Inc., for the U.S. Department of Energy’s National Nuclear Security Administration under contract DE-NA0003525.

REFERENCES

1. B. Hanson, H. Alsaed, C. Stockman, D. Enos, D., R. Meyer, K. Sorenson, “Gap Analysis to Support Extended Storage of Used Nuclear Fuel” FCRD-USED-2011-000136 (U.S. Department of Energy, 2012): p. 218.

2. R.M. Kain, “Marine atmosphere corrosion cracking of austenitic stainless steels,” *Materials Performance* 29,12 (1990): pp. 60-62.

3. C.R. Bryan, D.E. Enos, “Analysis of Dust Samples Collected from Spent Nuclear Fuel Interim Storage Containers at Hope Creek, Delaware, and Diablo Canyon, California” SAND2014-16383 (Albuquerque, NM, Sandia National Laboratories, 2014), p. 281.

4. EPRI, “Diablo Canyon Stainless Steel Dry Storage Canister Inspection” Technical Report #3002002822 (Palo Alto, CA, Electric Power Research Institute, 2016): p. 100.

5. Z. Chen, R. Kelly, “Computational modeling of bounding conditions for pit size on stainless steel in atmospheric environments,” *Journal of the Electrochemical Society* 157, 2 (2010): pp. C69-C78.

6. Y. Kondo, “Prediction of fatigue crack initiation life based on pit growth,” *Corrosion* 45, 1, (1989): pp. 7-11.

7. A. Turnbull, L. McCartney, S. Zhou, “A model to predict the evolution of pitting corrosion and the pit-to-crack transition incorporating statistically distributed input parameters,” *Corrosion Science* 48, 8 (2006): pp. 2084-2105.

8. A. Turnbull, “Corrosion pitting and environmentally assisted small crack growth,” *Proceedings of the Royal Society A: Mathematical, Physical and Engineering Science* 470, 2169 (2014): 20140254.

9. ASTM D1141-98, “Standard Practice for the Preparation of Substitute Ocean Water” (West Conshohocken, PA: ASTM).

10. T.W. Wolery, R.L. Jarek, “Software User’s Manual, EQ3/6 Version 8.0” (Albuquerque, NM: Sandia National Laboratories, 2003): p. 376.

11. SNL, “In-Drift Precipitates/Salts Model” ANL-EBS-MD-000045 REV 03 (Albuquerque, NM, Sandia National Laboratories, 2007): p. 358.

12. J. Deelman, “Low-temperature nucleation of magnesite and dolomite,” *Neues Jahrbuch Fur Mineralogie Monatshefte* 1999, 7 (1999): pp.289-302.

13. A.P.A. dos Anjos, A. Sifeddine, C.J. Sanders, S.R. Patchineelam, (2011), “Synthesis of magnesite at low temperature,” *Carbonates and Evaporites* 26, 3 (2011): pp. 213-215.

14. A. Nishikata, Y. Ichihara, Y. Hayashi, T. Tsuru, “Influence of electrolyte layer thickness and pH on the initial stage of the atmospheric corrosion of iron,” *Journal of the Electrochemical Society* 144, 4 (1997): pp.1244-1252.

15. J.O.M Bockris, A.K.N. Reddy, *Modern Electrochemistry: Ionics*. *2nd Edition*, (New York, NY: Kluwer Academic, 2002) p. 825.

16. V.L. Thurmond, R.W. Potter, M.A. Clynne, “The Densities of Saturated Solutions of NaCl and KCl from 10ºC to 105ºC” U.S.G.S. Open File Report 84-253 (U.S. Geological Survey, 1984): p. 10.

17. H.P. Eugster, C.E. Harvie, J.H. Weare, “Mineral equilibria in a six-component seawater system, Na-K-Mg-Ca-SO 4-Cl-H 2 O, at 25 C,” *Geochimica et Cosmochimica Acta* 44, 9 (1980): pp. 1335-1347.

18. C.E. Harvie, J.H. Weare, L.A. Hardie, H.P. Eugster, “Evaporation of seawater: calculated mineral sequences,” *Science* 208, 4443 (1980): pp. 498-500.

19. J. Usiglio, “Analyse de l'eau de la Mrditerranre sur les crtes de France,” *Annales Chim. Phys.* 27, (1849): pp. 2-107, 177-191.

20. J.H. Van't Hoff, “Zur Bildung zeanischer Salzblagerungen” 1st issue: (Vieweg, 1905): p. 85.

21 J.H. Van't Hoff, “Zur Bildung zeanischer Salzblagerungen” 2nd ed. (Vieweg, 1909): p. 90.

22. J.H. Van't Hoff, “Untersuchungen tiber die Bildungsverhaltnisse der ozeanischen Salzablage-rungen” (Leipzig: Akad. Verlags ges, 1912): p. 374.

23. M. McCaffrey, B. Lazar, H. Holland, “The evaporation path of seawater and the coprecipitation of Br^- and K^+ with halite,” *Journal of Sedimentary Research* 57,5 (1987): pp. 928-937.

24. M.J. Rossi, “Heterogeneous reactions on salts,” *Chemical Reviews* 103, 12 (2003): pp. 4823-4882.

25. D.R. Hitchcock, L.L. Spiller, W.E. Wilson, “Sulfuric acid aerosols and HCl release in coastal atmospheres: Evidence of rapid formation of sulfuric acid particulates,” *Atmospheric Environment* 14 (1980): pp. 165-182.

26. S.M. Wall, W. John, J.L. Ondo, “Measurement of aerosol size distributions for nitrate and major ionic species,” *Atmospheric Environment (1967)* 22, 8 (1988): pp. 1649-1656.

27. W.C. Malm, B.A. Schichtel, M.L. Pitchford, I.L. Ashbaugh, R.A. and Eldred, “Spatial and month trends in speciated fine particle concentration in the United States,” *Journal of Geophysical Research* 109, D3 (2003): pp. 1-22.

28. C.A. Pio, D.A. Lopes, “Chlorine loss from marine aerosol in a coastal atmosphere,” *Journal of Geophysical Research-Atmospheres* 103, D19 (1998): pp. 25263-25272.

29. B. Vierkorn-Rudolph, K. Bächmann, B. Schwarz, F. Meixner, “Vertical profiles of hydrogen chloride in the troposphere,” *Journal of atmospheric chemistry* 2, 1 (1984): pp. 47-63.

30. D. Möller, “The Na/Cl ratio in rainwater and the seasalt chloride cycle,” *Tellus B* 42, 3 (1990): pp. 254-262.

31. G. Harris, D. Klemp, T. Zenker, “An upper limit on the HCl near-surface mixing ratio over the Atlantic measured using TDLAS,” *Journal of atmospheric chemistry* 15, 3 (1992): pp. 327-332.

32. M. Kulmala, A. Toivonen, T. Mattila, P. Korhonen, “Variations of cloud droplet concentrations and the optical properties of clouds due to changing hygroscopicity: A model study,” *Journal of Geophysical Research: Atmospheres* 103, D13 (1998): pp. 16183-16195.

33. T.A. Crisp, B.M. Lerner, E.J. Williams, P.K. Quinn, T.S. Bates, T.H. Bertram, “Observations of gas phase hydrochloric acid in the polluted marine boundary layer,” *Journal of Geophysical Research: Atmospheres* 119, 11 (2014): pp. 6897-6915.

34. N. Fairweather, N. Platts, D. Tice, “Stress-corrosion crack initiation of type 304 stainless steel in atmospheric environments containing chloride: influence of surface condition, relative humidity, temperature and thermal sensitization,” *CORROSION 2008* (NACE International., 2008): paper 08485.

35. K. Shirai, J. Tani, T. Arai, M. Waturu, H. Takeda, T. Saegusa, “SCC evaluation test of a multi-purpose canister,” *Proceedings, 13th International High-Level Radioactive Waste Management Conference (IHLRWMC)*, (American Nuclear Society, 2011): pp. 824-831.

36. E. Schindelholz, B. Risteen, R. Kelly, “Effect of relative humidity on corrosion of steel under sea salt aerosol proxies I. NaCl” *Journal of the Electrochemical Society* 161, 10 (2014): pp. C450-C459.

37. E. Schindelholz, B. Risteen, R. Kelly, (2014). Effect of relative humidity on corrosion of steel under sea salt aerosol proxies II. $MgCl_2$, artificial seawater,” *Journal of the Electrochemical Society* 161, 10 (2014): pp. C460-C470.

38. NRC, “Assessment of Stress Corrosion Cracking Susceptibility for Austenitic Stainless Steels Exposed to Atmospheric Chloride and Non-Chloride Salts” NUREG/CR-7170 (Washington D.C.: U.S. Nuclear Regulatory Commission, 2014): p. 173.

39. E. Schindelholz, R. Kelly, “Application of inkjet printing for depositing salt prior to atmospheric corrosion testing,” *Electrochemical and Solid-State Letters* 13, 10 (2010): pp. C29-C31.

40. S. Suffield, J.A. Fort, J. M. Cuta, H.E. Adkins, “Thermal Modeling of NUHOMS HSM15 Storage Module at Calvert Cliffs Nuclear Power Station ISFSI” U.S. Department of Energy, (2012): pp.